An Automated Framework to Decouple pTx Arrays with Many Channels

Zohaib Mahmood[1], Bastien Guérin[2], Elfar Adalsteinsson[1,3], Lawrence L. Wald[2,3], and Luca Daniel[1]

[1]Dept of Electrical Engineering & Computer Science, Massachusetts Institute of Technology, Cambridge, Massachusetts, United States, [2]Martinos Center for Biomedical Imaging, Dept. of Radiology, Massachusetts General Hospital, Charlestown, Massachusetts, United States, [3]Harvard-MIT Division of Health Sciences Technology, Cambridge, Massachusetts, United States

Target audience: RF engineers and MR physicists. **Purpose:** In coupled pTx arrays, the power delivered to a channel is partially transmitted to other channels and partially dissipated in the circulators. As a result, for the same tradeoff between SAR and excitation fidelity, coupled pTx arrays require more input power compared to uncoupled ones. Ladder networks have been proposed for decoupling pTx coils, but are difficult to build and unreliable because of their high sensitivity to specific tuning and matching conditions of the array [1]. A secondary approach of pre-adjusting the low-power or digital waveforms would provide uncoupled B1+ array patterns, but would not solve the problem of lost power due to destructive interference at the ports of the array or loss of reflected/coupled power into the input of the RF amp or circulator. When the fate of reflected or coupled power incident on the RF power amps/circulators is considered, the system is not a simple linear system. In this paper, we propose an automated approach to design general high-power decoupling matrices interfaced between the RF amplifiers and the coil. Similar to a Butler matrix [2], the decoupling matrix mixes the input signals but is also optimized to ensure all forward power goes into the patient. **Method:** Given a pTx coil with N channels, we design a $2N$-port decoupling matrix placed between the RF amplifiers and the coil in a way similar to [3]. The decoupling condition for this matrix is $Z_{out} = Z_{11} - Z_{12}(Z_{22} + Z)^{-1}Z_{21}$ [3], where Z_{out} is the output impedance of the decoupling network at the source side. $Z_c = \{Z_{11}, Z_{12}, Z_{21}, Z_{22}\}$ is the unknown impedance of the decoupling matrix and Z is the impedance of the coupled pTx array. The decoupling condition is $Z_{out} = diag(50\Omega)$. We solve for an optimal decoupling matrix (Z_c) by minimizing the least-square objective function $\|Z_{out} - Z_u\|_2^2$. . Unlike [3], where the authors consider the special case $Z_{11} = Z_{12} = Z_{21} = Z_{22}$, we design Z in the most general way consistent with the condition that Z can be practically realized using passive and non-resistive components. The lossless condition is expressed mathematically as $\Re e\{Z_c\} = 0$. Symmetry, required for passive reciprocal networks, is expressed mathematically as $Z_{12} = Z_{21}^T, Z_{11} = Z_{11}^T, Z_{22} = Z_{22}^T$. To solve the problem numerically, we compute the cost function Jacobian $J = [I \otimes I \quad -I \otimes Z_{12}(Z_{22} + Z)^{-1} \quad -(Z_{22} + Z)^{-1}Z_{21} \otimes I \quad (Z_{12}^T \otimes Z_{12})((Z_{22} + Z)^{-T}(Z_{22} + Z)^{-1})]$. We tested our approach on a pTx 3T body coil with 16 channels distributed in 2 rows (Fig. 1). We used HFSS to compute the fields and the frequency response of this coil when loaded with the thirty-three tissue types Ansys body model. The coil was tuned (123.2MHz) and matched (-30dB) but was not decoupled [4,5]. **Results and Discussion:** Fig. 2 plots the norm of residuals depicting convergence (in about 150-200 iterations) of our algorithm for random initial guesses. The algorithm converges to distinct solutions depending on the initial guess. Non-uniqueness of the solution matrices allows specification of additional constraints such as limiting the capacitance and inductance values, and robustness of the solution matrix to external factors. Fig. 3 shows the structure of one of the solution matrices (Z_c). Z_{22}(lower right block) has a specific structure defined by the original coil assembly, where every coil is coupled to its neighbors. Fig. 4 and 5 show the nearly perfect decoupling (0=no coupling, 1=perfect coupling) that results from application of the decoupling matrix (S_{12} was reduced from ~-2dB to ~-200dB). Fig. 6 and 7 show L-curves corresponding to RF-shimming pulses designed (i) with the coupled array, (ii) the array decoupled using our decoupling matrix and (iii) the array ideally decoupled in simulation. Least-square pulses were computed while explicitly constraining local SAR and power [4]. They show that the coupled array was able to achieve a similar local SAR vs. fidelity tradeoff than the uncoupled ones however at the cost of greatly increased power consumption. There was no significant difference in performance between the ideally decoupled array and the array decoupled using our decoupling matrix. This also shows that the decoupling matrix produces mixed outputs that are non-degenerate and are therefore useful for pulse design (i.e., the singular values of the mixing matrix S_{21} are all of the same magnitude). **Conclusion:** We presented a framework to automatically design decoupling matrices for pTx arrays with many channels (>8). The algorithm optimally selects the decoupling matrix by enforcing reciprocity, passivity and the lossless-ness constraints on the network. We show that our algorithm converges and the decoupling matrix achieves near perfect decoupling. Note that we have not proposed yet a methodology for designing a circuit realizing the computed decoupling matrix using lumped elements. This is work in progress. Future work will include the development of a framework to automatically generate and compare different circuit topologies implementing the decoupling matrix.

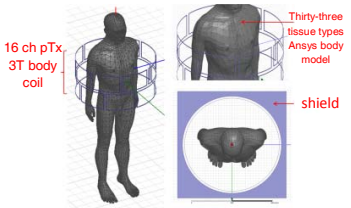

Fig. 1: EM simulation of a pTx coil with 16 channels distributed in 2 rows.

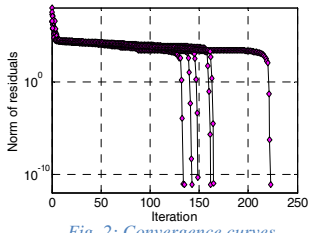

Fig. 2: Convergence curves

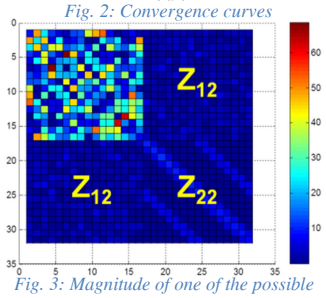

Fig. 3: Magnitude of one of the possible decoupling matrices

References: [1] Jevtic J (2001). Proc. ISMRM, **17**. [2] Alagappan V(2007). Proc. ISMRM **15**: 165. [3] Lee R (2002). MRM **48**(1): 203-213 [4] Guérin B (2012). Proc. ISMRM,**20**: 2612. [5] . Kozlov M (2009). JMR **200**(1): 147-152.

Acknowledgements: NIH support: R01EB0006847, R01EB007942.

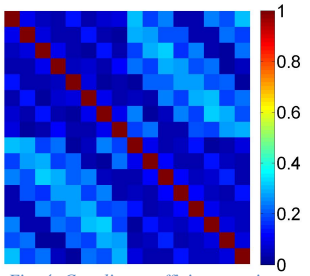

Fig. 4: Coupling coefficient matrix WITHOUT the decoupling network

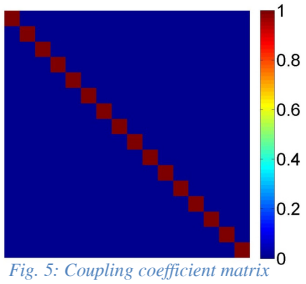

Fig. 5: Coupling coefficient matrix WITH the decoupling network

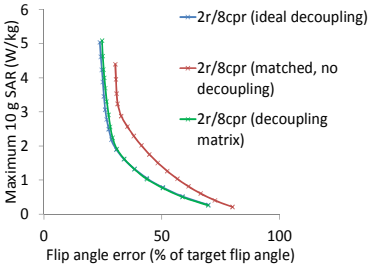

Fig. 6: Local SAR vs. fidelity L- curves (slice-selective RF-shimming)

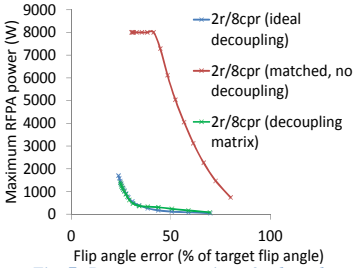

Fig. 7: Power consumption of pulses shown in Fig. 6